Journal of Civil Structural Health Monitoring (2021) 11:931–947
https://doi.org/10.1007/s13349-021-00488-7

ORIGINAL PAPER

Fatigue crack detection in welded structural components of steel bridges using artificial neural network

Maryam Mashayekhi[1] · **Erin Santini-Bell**[1] · **Saeed Eftekhar Azam**[1]

Received: 13 January 2021 / Revised: 1 May 2021 / Accepted: 4 May 2021 / Published online: 25 May 2021

Abstract
Under the cyclic traffic loads, welded structural components of steel bridges may encounter fatigue, which can cause a shorter service life and lead to fracture. A precise fatigue life prediction of structural components requires an accurate collection of stress cycles of the respective component. The density of sensors installed for monitoring the component and the distance to the concentrated stress areas are the features, which impact the efficacy of the estimated fatigue life. In this study, a platform is developed for the data-driven fatigue assessment of welded structural components of steel bridges, using artificial neural networks (ANN). The proposed algorithm is implemented for a case study, vertical lift truss bridge, the Memorial Bridge, Portsmouth, NH. A 12-month data collection period is utilized for the algorithm, from the long-term SHM program of the bridge. The stress cycles are used to estimate fatigue responses of an instrumented structural component of the bridge and determine the correlation between the estimated fatigue responses at the instrumentation plan. Additionally, a validated finite element model of the bridge is utilized to investigate fatigue responses in the unhealthy condition of the objective component. Therefore, multiple physical damage cases are simulated to compute the damage-induced stresses and the resulting fatigue life. The healthy and damaged fatigue responses are the ANN inputs, to detect crack-induced variation in the estimated fatigue responses at the instrumented locations. It is demonstrated that the proposed damage detection method can effectively detect possible fatigue cracks using a detailed database of damaged and healthy fatigue damage indices for training ANNs.

Keywords Crack simulation · Fatigue crack detection · Fatigue damage index · Traffic pattern · Artificial neural network

1 Introduction

Structural health monitoring (SHM) of civil infrastructure can play a significant role in mitigating unexpected structural failure by providing continuous health status reports of structures [1, 2]. Estimation of fatigue strength for fracture critical components is one of the significant applications of SHM data in steel bridges [3]. The accuracy of the resulting fatigue damage index is dependent on the cyclic stresses that are collected via the SHM system of the bridge. Because SHM sensors within a network are typically sparse, the sensors measure the strains at discrete locations, which can be far from the welded area [4]. Therefore, an emerged fatigue crack might not considerably influence the trend of collected stresses and the resulting fatigue damage accumulates. Consequently, the estimated fatigue remaining life of a structural component via field-collected SHM data may not precisely express the remaining service life of the cracked components [5].

In addition to the traffic loading impact, the field-collected structural responses include anomalies and outliers due to environmental variations [6]. False conclusions could be made through the estimated fatigue responses if the seasonal variations of stress responses are not well determined, though environmental variations may not significantly impact the estimated remaining fatigue life. Moreover, a validated finite element (FE) model can partially address the sparsity of sensors within a network and supplement the required data at the fracture critical locations for fatigue assessment [7]. Field-collected SHM data at the restricted instrumented locations of structures can be supplemented

✉ Maryam Mashayekhi
mm1182@wildcats.unh.edu

Erin Santini-Bell
erin.bell@unh.edu

Saeed Eftekhar Azam
saeed.eftekharazam@unh.edu

[1] Civil and Environmental Engineering, University of New Hampshire, Durham, NH, USA

with numerical crack tip structural responses to study crack propagation impact on the fatigue responses of a structural component. The integrated SHM data with numerical responses can provide a rich and efficient database which can be applied for fatigue crack detection in the long-term service life of bridges.

For autonomous and early detection of fatigue cracks, a machine learning approach is required as the changes in measured strain time histories prove to be subtle. Artificial neural networks (ANNs) are nonlinear mappings which use multiple interconnected neurons to predict the correlation between a set of input and output parameters [5, 8]. ANN methods are extensively applied for damage detection studies, using field SHM data and/or numerical responses as inputs [9–11]. In recent studies, ANNs have been used for fatigue damage detection of welded components in different structural types [12]. Kang et al. applied an ANN model for fatigue damage detection under multi-axial loading, using numerical data of an FE model [13]. Fathella, et al. used an ANN for fatigue crack detection of bridge decks, considering multiple crack scenarios [14]. Durdulae developed an ANN-based pattern for fatigue damage detection of steel components under random loadings in vortex-induced vibration. The developed pattern considered multiple parameters, including moments, ultimate tensile strength and fatigue strength coefficient, and exponent [15]. Zhan and Li developed an ANN-based tool for fatigue damage detection, considering additive manufacturing parameters for a specific printed material (SS 316L), using experimental data [16]. Ragheb et al. applied an ANN method for fatigue damage detection in steel railway bridges considering modeling uncertainties for multiple train loads [17]. Yan et al. utilized an ANN for probabilistic fatigue failure of bridges under overloaded traffic for a steel girder bridge using numerical data of a validated FE model [18]. Leander used an ANN model to predict fatigue life, using 1 year of collected SHM data for a railway bridge [19]. Xu et al. applied a deep convolutional neural network for the detection of fatigue cracks in steel bridges, using the images of crack samples of a bridge [20]. Wang et al., using a numerical model which was verified with experimental results, applied an ANN to determine fatigue crack growth directions for mixed-mode curved fatigue cracks under variable amplitude load [21].

In this study, an algorithm is proposed to evaluate the performance of the instrumented sensors in detecting possible fatigue cracks of welded structural components of steel bridges using long-term SHM data and an ANN. The SHM data are used to calculate the remaining fatigue lifespan at the instrumented locations of a welded component. The correlation between estimated fatigue responses in the healthy and damaged conditions of the instrumented structural components is determined using ANN. The proposed method is validated using a case-study bridge, the Memorial Bridge in Portsmouth, NH, that has a large SHM dataset due to permanently installed sensors. The bridge also includes a complex structural component, the gusset-less connection, which is selected for the fatigue crack detection goal of this study.

In addition to the SHM data, a validated FE model of the bridge is utilized to acquire knowledge about crack propagation stress variations and the resulting fatigue responses under variable amplitude traffic loads. Multiple fatigue cracks, varying in size and location, are simulated through the FE model. A stepwise crack propagation is also implemented in the FE model under different dynamic traffic loads. The data-driven healthy and numerical damaged (cracked) fatigue responses are the inputs to the ANN, which is then used to determine the minimum size of the crack that can be detected via the installed sensor network. This damage detection work relies on adopting a refined, calibrated model of the bridge and generating a rich and realistic set of training data for the ANN. In doing so, a novel multiscale FE model of the case-study bridge was utilized. The standard ANN coupled with field data and realistic damage scenarios from a large scale, iconic bridge can provide the researchers and practitioners insights into real-world potentials and the limitations of machine learning and physics-based models for SHM and decision making.

2 Methodology

2.1 Fatigue assessment

Fatigue strength of a structural component can be computed through the field collected SHM data, which are obtained from the installed sensors at the component. The time-history strain responses of strain rosettes are post-processed for fatigue assessment. As the linear elastic relationship is valid, the collected strain responses are converted into stress responses. The stress cycles at the structural components of bridges have a variable property, given the variable pattern of traffic programs in bridges. The cycles of variable amplitude stress ranges are extracted from the time-history stress responses. In this study, the Rainflow cycle algorithm is used for this purpose [22]. Miner's rule is then utilized to compute the fatigue damage index by superposing the cycles of variable amplitude stress ranges, which is expressed in Eq. (1) [23]. Fatigue damage index, D, is a ratio, varying from 0 to 1 that reflects the fatigue damage level of an investigating component:

$$D = \sum \frac{n_i}{N_i}, \tag{1}$$

where n_i denotes the number of collected stress cycles and N_i represents the number of remaining cycles to failure. The

N_i is determined in terms of fatigue properties of the material and the mean stress, S_{ai}, as expressed in Eqs. (2) and (3)

$$S_{ai} = \alpha_i c N_i^b, \tag{2}$$

$$\alpha_i = \left(1 - S_{mi}/S_{\mathrm{UTS}}\right), \tag{3}$$

where c and b, respectively, are the fatigue strength and exponents values for the material, based on stress amplitude. The mean stress parameter α_i in Eq. (2) is Goodman's correction factor to consider the effect of the mean stress, $S_{mi,}$ and roots in the ultimate strength of the material, S_{UTS}. The frequency domain expression, $N_{i,}$ can be determined through the appropriate S–N curves for an investigating component, recommended by AASHTO [24].

Additionally, crack tip structural responses are required to be determined to estimate the remaining fatigue life of the cracked components. If using an FE model, the details of a detected crack of the investigating structural component shall be considered in the FE model. The detected crack must be accurately modeled to obtain the numerical crack tip stresses. Fatigue remaining cycles of a cracked component can be computed through Paris law, expressed in the following equation [25]:

$$\frac{\mathrm{d}a}{\mathrm{d}N} = C(\Delta K)^m, \tag{4}$$

where C and m are material properties. da defines the crack length increment and dN refers to the number of cycles to failure corresponding to the crack length. da/dN expresses the rate of crack growth, which is the instantaneous slope of the crack growth curve. ΔK is defined as the stress intensity factor (SIF) that changes with crack increment.

2.1.1 Fatigue cycle estimates using SHM data

The fatigue strength for structural components of an in-service bridge can be estimated over discrete periods of data collection, using the long-term SHM data. An exclusive data collection period helps to study the trend of the estimated fatigue damage indices in the long-term service life of a bridge. The period is required to include the frequent stress ranges experienced by the structural components of the bridge. The choice of the optimum data collection interval depends on the traffic pattern and the structure's performance. The fatigue damage index may also have a variable trend due to the seasonal impacts, when the traffic pattern of the bridge is considerably correlated with the seasonal variations [26].

Besides, scattered traffic conditions are another source of variability in the recorded responses. Removal of the less influential stress cycles can reduce the computation time in calculating the fatigue damage indices. Therefore, less-frequent stress ranges (below 1% of total stress cycles experienced at the bridge) are removed from estimating fatigue damage indices. Low-amplitude stress ranges may occupy a significant portion of the field-collected data. These stress ranges are induced by the lower class of vehicles (class 1–5), or recorded data during light traffic time (based on traffic data records). The low-amplitude stress ranges may not impact the estimated fatigue damage indices, and therefore, are removed from the analysis. Also, before computing the fatigue damage index, the existing outliers due to the random noise or malfunction of the sensor must be removed from the collected SHM data. The outlier removal, in this study, is performed using the filtering toolbox in MATLAB.

2.1.2 Fatigue cycle estimates using numerical analyses

Application of SHM data for fatigue assessment of welded structural components is restricted to the instrumented locations of the structural component. Fatigue prone welded structural components are often less accessible areas for instrumentation. Consequently, the crack tip stress concentration may not be reflected in the fatigue damage index, which is estimated using the long-term SHM data. Alternatively, through a validated FE model, numerical stress responses at the desired stress-concentrated locations can be utilized for fatigue assessment. A validated FE model can also incorporate the traffic details, including the frequency and class of vehicles. The traffic scenarios can be simulated through a validated FE model of bridges, as dynamic moving loads. However, due to excessive computation time for analysis, only the major traffic conditions of a bridge shall be simulated via the FE model. The resulting numerical stress ranges are used to estimate fatigue damage index, using Eq. (1). The required stress cycles can be counted through the SHM data or traffic information of the bridge [27].

The model-based fatigue assessment method provides knowledge on structural performance of the concerning components to determine the fatigue category in estimating the remaining fatigue life of the component. A validated FE model also allows obtaining stress responses at the desired locations of structural components for estimating fatigue life of the component. In addition, the FE model aids to investigate propagation of the crack and the impact on the remaining fatigue life of the structural component. If the concerning structures do not include any reported crack, a possible crack can be simulated via the FE model, based on the assumptions on the location and characteristics of the crack. In this study, both the numerical healthy and damage-induced stress responses are utilized for the crack detection scope of the paper.

2.2 Artificial neural network

ANN is a mathematical tool that can be used for predicting the behavior of a system through a learning stage, which is the process of finding the weights and biases of a set of inter-weighted regression functions, namely, the neurons [28]. In this study, a Multilayer Perceptron (MLP) is adopted for fatigue crack detection. MLP is a back-propagation algorithm that trains the networks to link the nodes of the input layer, to the nodes of the output layer [29]. The relationship between the input and output through a neuron i can be expressed as follows:

$$y_j = f_i\left(\sum w_{ij}x_j - t_i\right), \tag{5}$$

where x_j are the inputs of the network that are multiplied by the weights, w_{ij}. y_j is the output of the network, which is computed through an activation function f_i, when the sum of the weighted inputs $w_{ij}x_j$ are higher than a threshold t_i.

2.3 The proposed fatigue crack detection algorithm

A stepwise procedure for crack detection is shown in Fig. 1. In the beginning of the algorithm, it is required to locate the fatigue prone locations of the bridge, regarding the inspection reports of the bridge. Long-term SHM data are required to be collected through the installed sensors at the investigating structural component. The period of data collection needs to be long enough to incorporate the dominant traffic loads at the bridge and capture environmental variabilities. The collected long-term SHM data is subsequently divided to several shorter periods with similar duration. The unique duration of field data is determined based on the recorded stress variations at the objective structural component. For each small period, the SHM data are post-processed to extract cycles of recorded stress ranges for estimating fatigue damage index through Miner's rule. In addition to SHM data for each period, additional information needs to be collected, which include environmental data to input ANN. An average temperature and wind speed were considered for these estimated fatigue damage indices. In the next step, fatigue damage indices of the damaged structure are estimated, which is required for the ANN input. In this algorithm, damage stresses are obtained via numerical efforts to estimate fatigue damage index of the damaged component. A validated FE model is applied to simulate fatigue cracks and extract crack tip time-history stresses under dynamic traffic loads on the model. The traffic load information of the bridge shall be acquired from field observations to precisely define the truckloads in the FE model. Crack type and locations are either obtained from the inspection report or simulated at fracture critical locations of the component. The numerical crack tip stresses in this step are utilized to calculate fatigue damage indices of the damaged component (D_{crack}). The estimated healthy and damaged fatigue damage indices as well as the additional data (environmental) are input to ANN for training. The damage detection results are extracted from ANN.

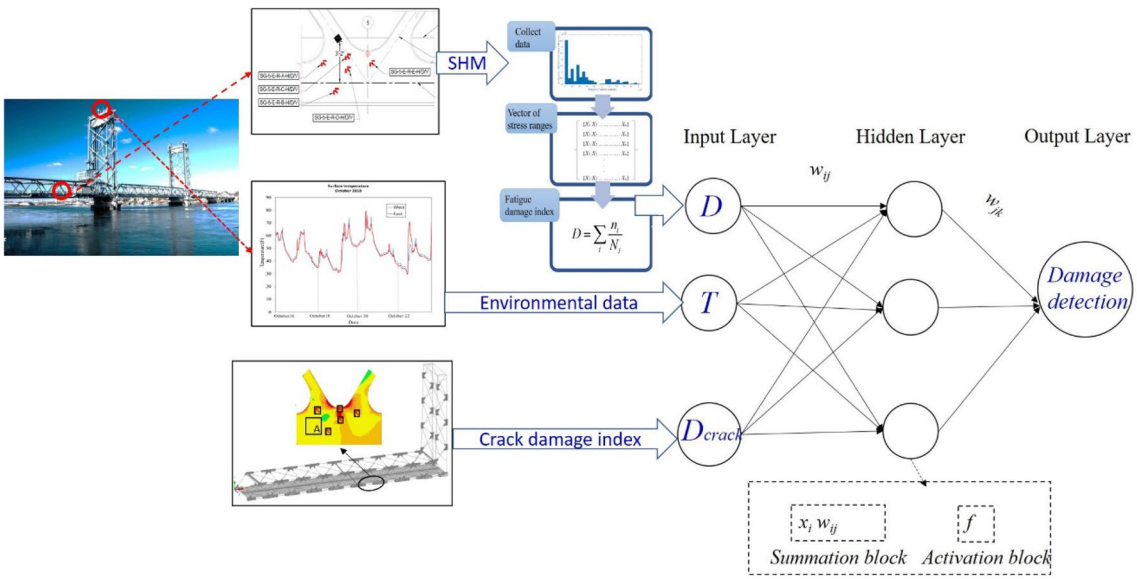

Fig. 1 The procedure to develop a NN model for fatigue crack detection

3 The case-study bridge

3.1 Details, design, and construction

The case study in this research is the Memorial Bridge, a steel vertical-lift truss bridge in Portsmouth, NH, that connects the two states of NH and ME, as shown in Fig. 2 [30, 31]. The bridge was inaugurated to vehicular and naval traffic in August 2013. The bridge consists of three spans and two towers. The two fixed and one movable span have the identical size of 90 m length, and 15.24 m width. The two identical towers have the height of 42 m. The bridge includes a novel gusset-less connection, which has a specific complex web geometry and cold-formed bent flanges shown in Fig. 2b. The bent flanges of the connection are connected to the, web through curved fillet welds, with 15. 85 mm size. The complex geometry of the connection and the weld create an exclusive structural performance, which is reflected in the structural responses. Given the complex performance of the connection, this study focuses on fatigue crack detection at the gusset-less connection through integrating field collected SHM data of the connection and numerical results of an FE model of the bridge. The long-term SHM program and FE model of the bridge are explained in the following.

3.2 Long-term SHM program of the bridge

A long-term SHM program was designed for the Memorial Bridge, which has been started to operate, since March 2017. The sensors are instrumented at the south span and south tower of the bridge to provide continuous real-time data at the critical locations of the structure. The SHM instrumentation plan includes 16 strain rosettes, 2 uni-axial strain gages, 12 uni-axial accelerometers, 4 tiltmeters installed at multiple locations of the bridge to provide continuous data for condition assessment, design verification, and decision-making program of the bridge [31].

Fatigue assessment of the gusset-less connection is one of the main objectives of the SHM program of the bridge, which contributes to the maintenance programs of the bridge. In addition, the complex geometry of the gusset-less connection does not fit in the documented fatigue categories in the available design codes [24]. Therefore, fatigue assessment of this novel gusset-less connection provides insights on this new design approach. An array of five strain rosettes is installed at multiple locations of the top chord and bottom chord gusset-less connection to precisely understand the local performance of the connection (shown in Fig. 2). The current inspection results did not report any detected damage. Therefore, no information is available about the damage-induced stress responses. The complex structural response distribution and fatigue performance of the gusset-less connection motivate to implement the proposed algorithm of this study for fatigue crack detection of this component.

4 The data-driven fatigue damage index

In this section, the procedure for data-driven fatigue damage indices is expressed which include field data collection, post-processing of the data, and calculation of fatigue damage indices. The data are collected from the healthy condition of the gusset-less connection.

4.1 Long-term field data collection

In this section, time-history strain responses of the five installed strain rosettes at the bottom gusset-less connection

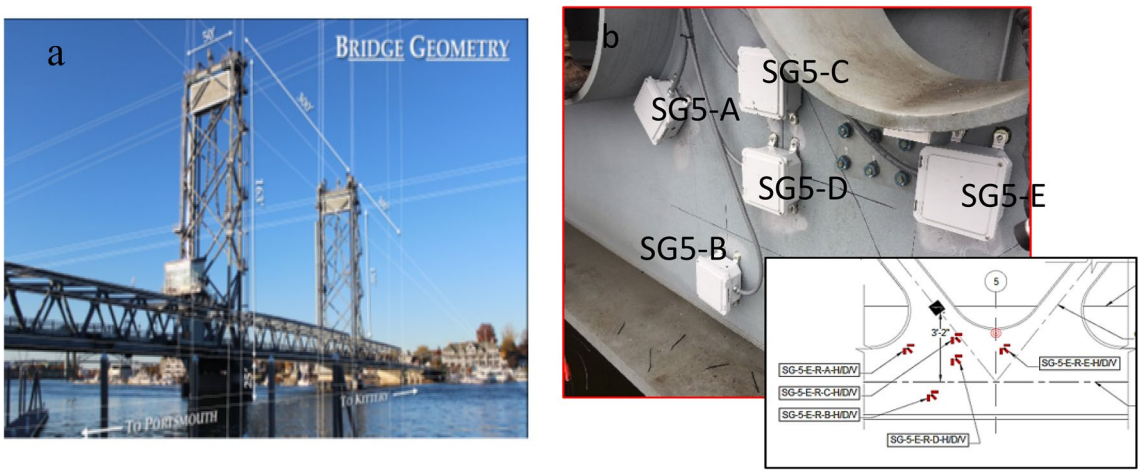

Fig. 2 The Memorial Bridge, Portsmouth, NH (**a**), The gusset-less connection of the Memorial Bridge (**b**)

(as shown in Fig. 2) are collected to estimate the fatigue damage index. In Fig. 3, the horizontal, vertical and diagonal time-history strain responses of the five strain rosettes are used to show a representative of principal strain time-history for the strain rosettes, SG-A to SG-E, which are shown with letters A–E, respectively. It is observed that the recorded strain responses at locations A, C, D, have a similar trend, while the strain response of the SG-B is different. The SG-E is significantly influenced by the floor beam, which is directly located close to the strain rosette. In addition, SG-A is close to the side curve weld of the gusset-less connection, which may reflect the concentrated strains at this welded area. However, all the recorded strain responses report a similar cycle count. A fatigue crack may be captured by one or more of these strain rosettes, depending on the size and location of the fatigue crack.

The recorded time-history strain responses require some preprocessing to calculate fatigue damage index. Given the linear elastic performance of the structure, the field-collected strain responses are transferred into principal stresses, using the elasticity modulus (200 GPa), which was considered in the design of the bridge. In addition, before computing the fatigue damage index, the existing outliers must be removed from the collected data. These outliers are either induced by random noise or malfunction of the sensor. In this study, the filtering MATLAB toolbox is used for outlier removal. Subsequently, the time-history strain responses are transformed to variable amplitude stress ranges using the Rainflow cycle algorithm [22]. The extracted stress range/cycles of a period of data collection are used to exclusively calculate the fatigue damage index for each strain rosettes.

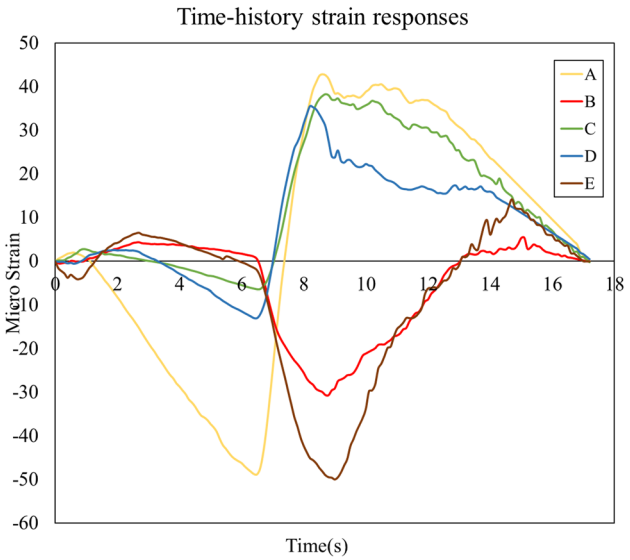

Fig. 3 Time history strain responses of the five strain rosettes

4.1.1 Time interval for field data collection

To calculate the fatigue damage index, an ample period is required to ensure the frequent traffic loads are included in the response. The traffic load variations can be associated with seasonal changes or the changes in the traffic program of the bridge, which result in a fluctuating trend for the calculated fatigue damage indices. The fatigue damage index depends on the number of cycles and stress amplitudes, which are the major sources of variability of the responses estimated in different periods. This variability of the fatigue damage indices can adversely impact fatigue crack detection. Therefore, in this section, a consistent time-interval is defined for the estimated fatigue indices, in the long investigating period of data collection.

The unique consistent intervals can remove the impact cycle number on the estimated fatigue damage indices. Therefore, the variability of fatigue damage index with the stress cycle changes was studied to determine the appropriate duration of data collection. In this study, 12 months of measured sensor data from the Memorial Bridge was investigated to select the duration of the time window, required for capturing the statistical features of traffic induced stress cycles. Fatigue damage indices were estimated using Miner's rule, expressed in Eq. 1. The lower strain responses that were recorded under the lightweight traffic were excluded from the data collection periods. Only strain cycles above 20 micro-strains were included in the analysis. In some published literature, 20 με was adopted by engineering judgement to be a suitable threshold for excluding signals in fatigue damage detection analyses [32, 33]. Therefore, the duration of the period was defined based on the cycles of high-amplitude strain ranges. The duration of periods was expressed as the truck events, since the higher amplitude strain ranges are frequently induced under the heavy truck passages.

In Fig. 4, the trend of fatigue damage index with sequential truck events is depicted for four different periods. The four considered periods were chosen to start at four different seasons of the year with similar truck events. Therefore, the selected periods coincide at the end of the period. It is demonstrated that the four graphs have a fluctuating trend at the beginning of data collection, while the difference between the fatigue damage indices is considerable. As the number of truck events reaches a specific level, each graph's trend begins to plateau and the discrepancy between the estimated fatigue damage indices becomes marginal. It is also illustrated that the sufficiency points for the selected periods may not be identical. However, a period of about 600 truck events, seems to be a reasonable interval, which is selected as the exclusive period of data collection. In this study, the 12-months collected time-history strain responses of five strain rosettes are utilized. The 12-month data collection

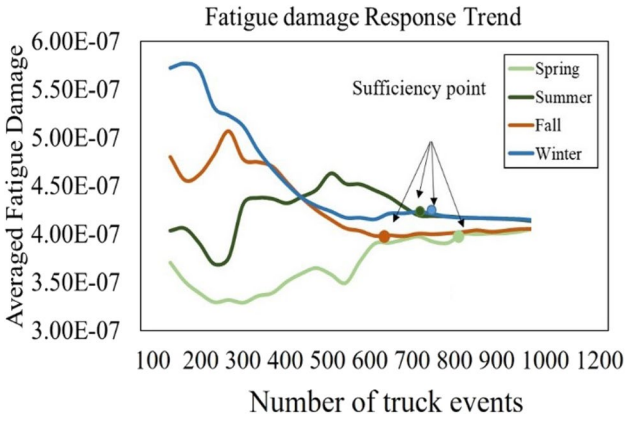

Fig. 4 Trend of averaged fatigue damage index versus truck event cycles for four periods

period is divided into multiple periods with a unique duration of 600 truck events, and fatigue damage index is estimated for each period.

4.2 Fatigue damage index estimation

Based on the performance of the gusset-less connection and the designer's assumption, fatigue category B is assumed for estimating fatigue damage index, using the field collected data. Fatigue Category B is a terminology adopted by AASHTO Design Manual with allocated S–N curve. Category B represents the continuous fillet weld parallel to the direction of applied stress [24]. The recorded time-history responses of the strain rosettes are post-processed to obtain the stress ranges, and associated cycles, via the Rainflow cycle algorithm. Using the stress range/cycles of a period of data collection, the fatigue damage index is exclusively calculated for the five investigating strain rosettes. The resulting indices become only dependent on the amplitude of collected stress ranges, due to the equal cycle counts. The stress ranges and resulting fatigue damage indices may still reflect the traffic pattern changes, seasonal variations, ambient noise, and measurement errors. However, the structural effects of excessive crack tip stresses may be better reflected in the resulting fatigue damage index, which improves the fatigue crack detection procedure.

In Fig. 5, the average monthly collected fatigue damage indices are shown for the 12 months of data collection at strain rosette SG-A. The graph demonstrates the variability of the estimated fatigue damage index, using field collected SHM data. It is observed that the fatigue damage index has a variable mean value in different seasons, while less variability is observed within each season. Therefore, in a long-term SHM program, application of a consistent period causes a more predictable trend for the estimated fatigue damage indices. Consequently, the damage-induced changes can be detected more efficiently through the estimated trend of the fatigue damage index.

The calculated fatigue damage indices from the measured signals of the strain rosettes express the healthy conditions of the structure, as there was no damage observed during the period in which the data were being collected. Therefore, a high fidelity and computationally efficient numerical model was used for simulating the bridge response to the truck events, in the presence of fatigue cracks.

5 Computational model of the Memorial Bridge: bridge response in the presence of fatigue cracks

In this section, an FE model of the Memorial Bridge is used to obtain the numerical structural responses that are required for calculating fatigue damage index in the healthy and damaged conditions of the gusset-less connection.

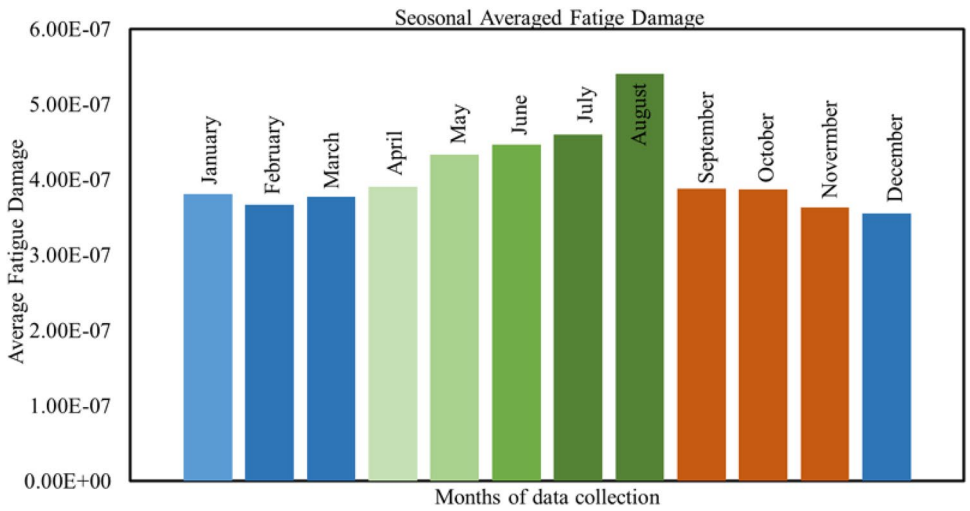

Fig. 5 Monthly averaged fatigue damage index for 12-month period of data collection at SG-A

5.1 FE model development

The FE model shown in Fig. 6 is created in LUSAS, an FE software package, which is appropriate for modeling the bridges. The model includes the instrumented part of the bridge (south span and south tower). As shown in the figure, the structural members are modeled with three-dimensional thick beam elements and three-dimensional eight-noded thick shell elements [33]. The shell element provides stress contour responses along the structural members to determine the stress concentrated areas, which are prone to fatigue crack initiation. The properties of the FE model are expressed in Table 1.

The created FE model is validated using the measured responses of the bridge during quasi-static and dynamic live load tests [34]. The simulated time-history responses are dependent on multiple uncertain modeling parameters, including element type, size, mesh layout, unintended rigidity induced by nonstructural components, and material property. Calibrating the FE model with the dynamic load tests can ascertain the accuracy of the numerical time-history stress responses for calculating fatigue damage index. In Fig. 7, the numerical and field-collected time-history stress responses are compared for SG-A under a single truck (Fig. 7a) and multiple trucks (Fig. 7b). It can be observed that the numerical and field-collected responses are in good agreement for the two traffic scenarios. At the same time, the difference may not impact the stress ranges and the resulting fatigue damage index.

The calibrated FE model is utilized to extract the required numerical time history responses at the location of the five strain rosettes for the healthy and damaged conditions of the structure. Traffic scenarios of the bridge are simulated to utilize the resulting numerical stress responses for estimating fatigue damage index. The simulated traffic scenarios of the bridges can result in. the numerical stress responses, which are consistent with the field-collected stress responses. Simulating all of the experienced traffic scenarios of the bridge can cause excessive computational cost for this study. Therefore, the simulated traffic scenarios are restricted to the dominant stress ranges of the bridge with high amplitude and frequency.

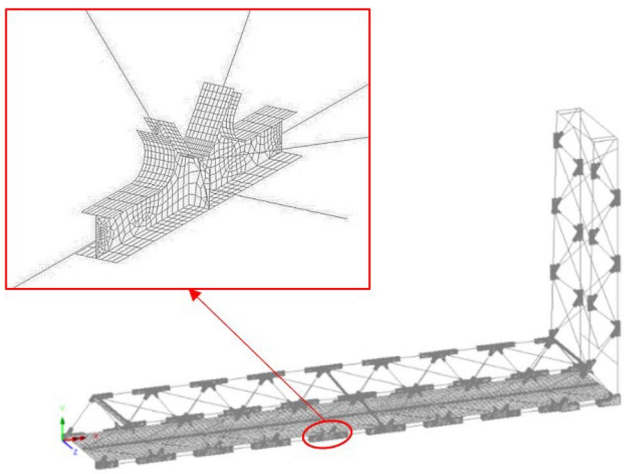

Fig. 6 The FE model of the Memorial Bridge in LUSAS

Table 1 The properties of FE model of the Memorial Bridge in LUSAS

Parameter	Quantity
Shell element number	158,993
Beam element number	5,160
Steel modulus of elasticity	200 GPa
Elasticity modulus of concrete	16.5 GPa
Poisson's ratio	0.3
Shell element sizes (max, min)	2.5,7.5 cm
Beam element sizes (max, min)	5,10 cm

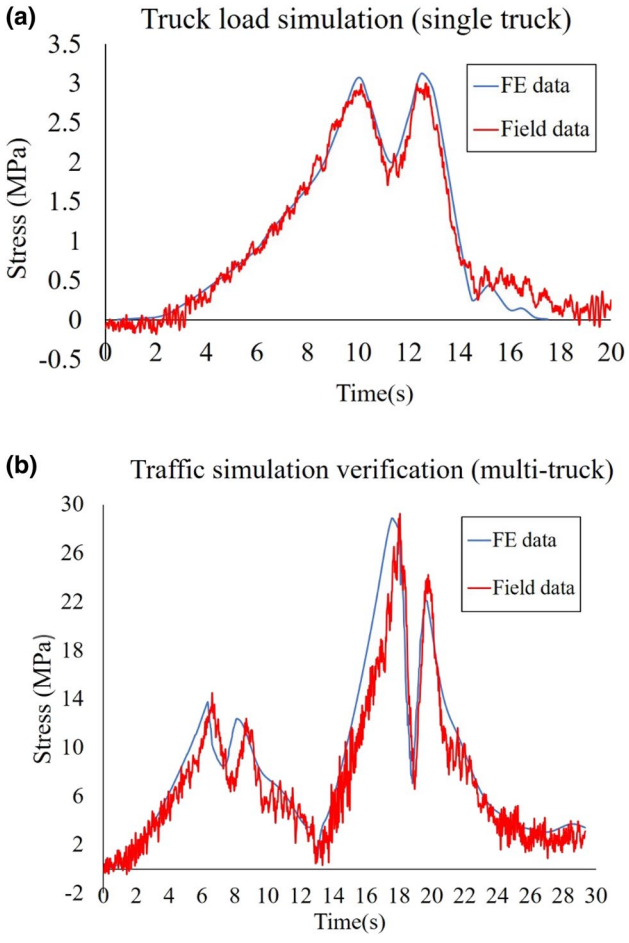

Fig. 7 Numerical and field-collected stress time-history at SG-A for **a** single truck, **b** multiple trucks

The information about the traffic patterns and truck counts are obtained from Annual Average Daily Traffic (AADT) information, which is reported by NHDOT and the traffic camera of the bridge. The axle load of each truck is applied to the deck of the model as a point moving load, with the constant speed of 45 km/h, traveling at the northbound, southbound, or two bounds of the bridge [35]. The cycle count information for estimating fatigue damage index is also based on the reported AADT data. In Table 2, seven simulated traffic scenarios are explained which may occur in the northbound (NB), southbound (SB) or both (NS). The number of trucks for each traffic scenarios is also expressed. The resulting fatigue damage indices are expressed for the five strain rosette locations, which represent the healthy condition of the structure. In the next section, the procedure for modeling fatigue cracks and calculating damage-induced structural responses are discussed.

5.2 Simulating fatigue crack via calibrated FE model

The fatigue cracks are often initiated at the high-stressed welded locations. Imperfections and the structural discontinuities at the welds can significantly increase the local stress concentrations and hence, the potential for crack initiation. In this section, fatigue crack is simulated at the high-stressed locations, at the weld toes of the gusset-less connection. Most of the available literature implements damage as the reduction of stiffness, thickness, or change in material properties of the FE models [36]. In complex structural components, there is a lack of data regarding structural responses in presence of various sources of damage [37]. As a remedy, structural responses in presence of damage can be obtained, using high-fidelity numerical simulations of fatigue cracks. Using stress state at the crack tips through fatigue crack simulations results in more precise fatigue damage indices of damaged structural components.

In this section, fatigue cracks are simulated via three-dimensional shell elements [37]. Small sizes of fatigue cracks are selected for simulation, since the current study seeks to detect the possible cracks, at the early stages. The available literature has multiple recommendations for initial crack sizes [38]. In this study, a minimum size of 12.5 mm is selected for crack initiation due to the considerable thickness of the gusset-less connection web (31.75 mm). The initiated crack is propagated to a 125 mm crack size, with 12.5 mm increments, to study the stress response variations due to crack growth. For each crack step, the moving loads are applied to the FE model, and the stress time histories are extracted at the five strain rosettes location. Also, the crack propagation direction is determined based on the principal stress directions at the crack tip, which is determined via the FE model results [39].

Three locations at the connection are selected for crack simulation, as shown in Fig. 8. The cracks are simulated at stress-concentrated locations along with the weld toes of the gusset-less connection. Two of the cracks are implemented at a close distance to the instrumented strain rosettes. The third crack is simulated at the interior stiffener of the gusset-less connection. The mesh sizes are adjusted in the vicinity of the cracked area ranging from 2.5 to 25 mm. Every crack case is modeled in a unique FE model, while the crack sizes are increased for each crack case. Consequently, three crack scenarios are simulated via the FE model, which include locations 1, 2, 3 in Fig. 8.

The numerical structural responses are obtained for each step of the crack size. Figure 9 displays the stress contour results of the gusset-less connection for the three crack cases. The figure shows the maximum size of the simulated cracks. It is seen that simulated cracks cause a higher stress amplitude around the cracked area, which may be reflected at the stress responses of one or more strain rosette locations.

Multiple traffic scenarios are considered for crack propagation. Lightweight traffic conditions (scenarios 1–4) were not applied to the model during crack propagation. The applied loads are required to result in the high amplitude stresses such that the crack is triggered to propagate [40]. In Fig. 10, an example of time-history principal stress responses is shown for the three cracks cases, under the traffic scenario 3 trucks-NB.

The resulting numerical crack tip time-history stress responses are utilized for fatigue damage estimation. The required cycle quantities are obtained from the collected SHM data. In Fig. 11, the range of estimated fatigue damage indices is shown for the five strain rosette locations, considering all of the crack sizes for the three crack cases. It is seen that the fatigue damage indices have more variability for SG-A and SG-E, as compared to the other strain rosette locations. The fatigue damage indices calculated, using the signals from healthy and damaged structure, which are integrated for training, validation and testing process via the ANNs, which is discussed in the next section.

Table 2 Fatigue damage index for simulated traffic scenarios

Traffic scenario	Fatigue damage index (10^{-6})				
	SG-A	SG-B	SG-C	SG-D	SG-E
1 truck-SB	3.35	2.93	3.80	3.61	5.48
1 truck-NB	7.61	6.95	9.83	6.66	12.1
2 trucks-NS	8.34	7.51	10.30	7.85	15.8
4 trucks-NS	13.21	11.84	15.79	12.82	17.95
6 trucks-NS	35.93	31.81	36.37	34.05	38.69
3 trucks-SB	28.73	24.64	29.16	27.88	30.22
3 trucks-NB	32.85	28.78	33.48	32.06	35.44

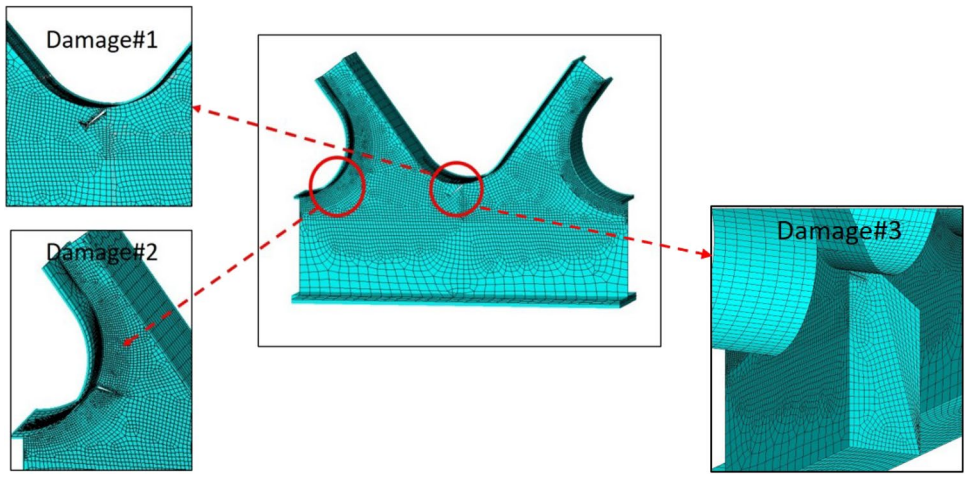

Fig. 8 The simulated fatigue cracks at the gusset-less connection through FE model in LUSAS

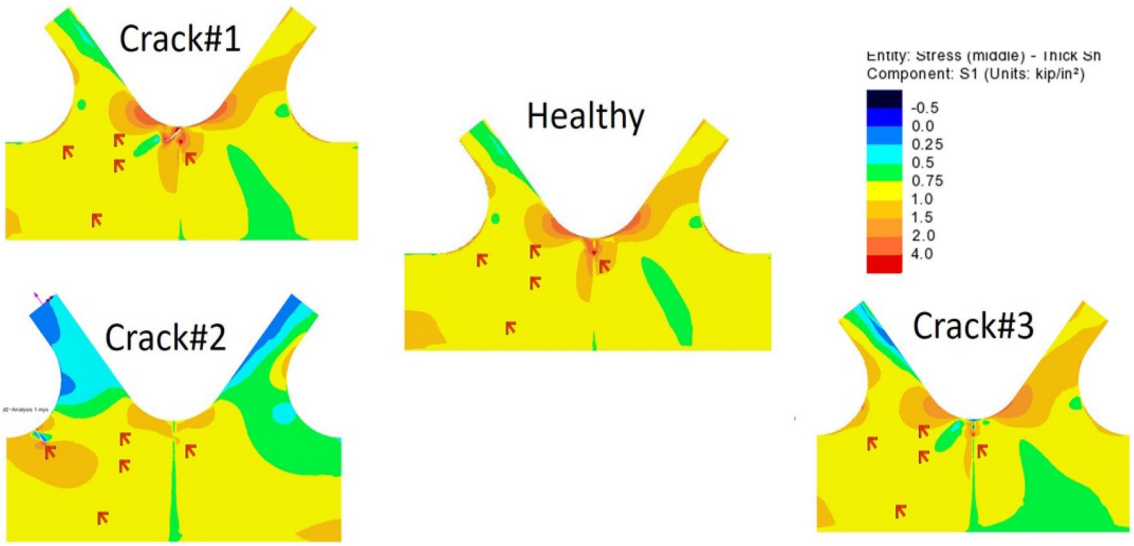

Fig. 9 The stress contours of the gusset-less connection healthy and three crack cases

6 ANN for fatigue crack prediction

6.1 Training process of fatigue damage index responses

In this section, the calculated fatigue damage indices, which are obtained from the field-collected data and the numerical responses of the validated FE model, are used for training the ANNs. The healthy fatigue damage indices are calculated using the field-collected data and the simulated numerical time histories at the location of these strain rosettes. The fatigue damage indices of the unhealthy structure are estimated using only the numerical time histories obtained from the cracked FE model. The healthy and cracked fatigue damage indices, which vary depending on crack location and size, as well as the additional information about the crack location and sizes, are the inputs to train the ANNs [41].

In Table 3, the number of samples used for training, validation, and testing of the ANNs is summarized. The estimated fatigue damage indices are labeled into three different categories, which are healthy, healthy-cracked, and cracked. It is noteworthy that for the healthy-cracked category, half of the stress cycles belong to healthy conditions, with the remainder of the stress cycles being extracted from early-stage crack initiation (12.5–50 mm crack size) and consisting of 300 samples of fatigue responses. In the cracked category, all stress cycles belong to the crack propagation process, which contain 400 samples of fatigue responses. The healthy-cracked category represents the insignificant changes in the calculated fatigue damage indices as

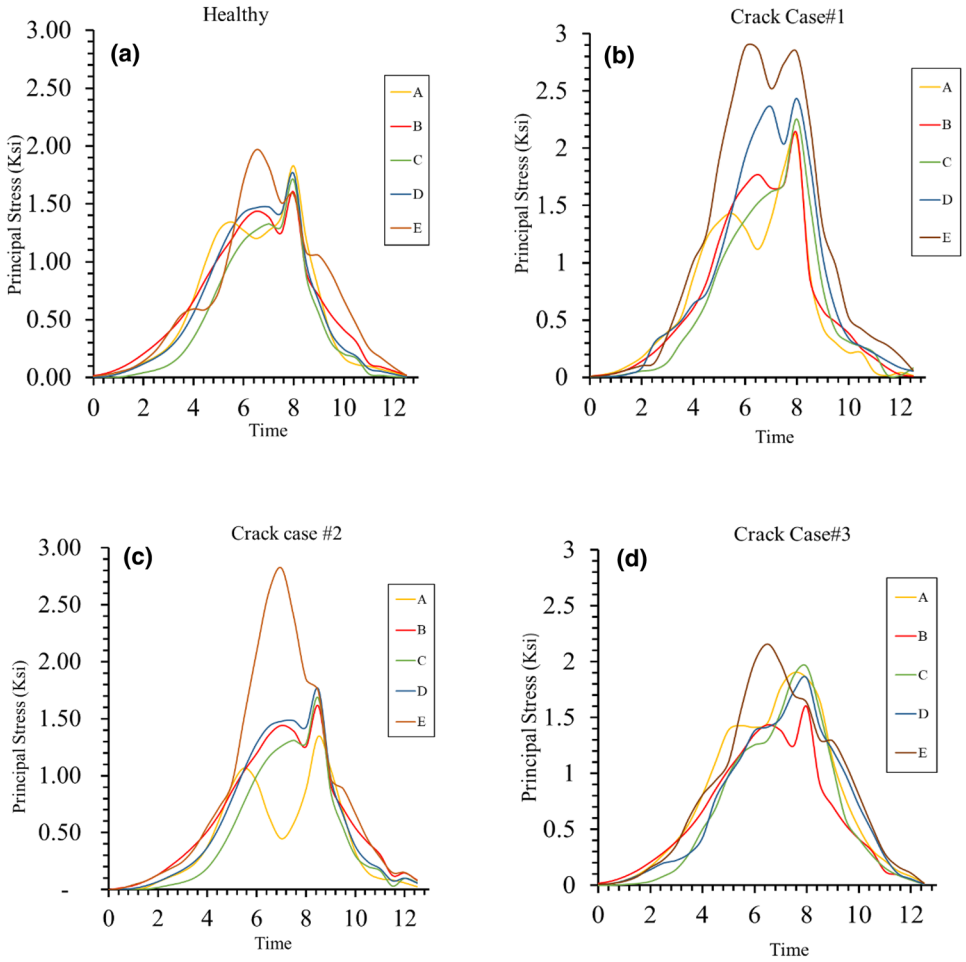

Fig. 10 Numerical time-history principal stress responses under the dynamic moving loads for **a** healthy, **b** crack case#1, **c** crack case #2, **d** crack case #3

compared with cracked category. The input data is divided into approximately 70%, 15%, and 15% for training, validation, and testing, respectively. The ANNs are constructed using the Neural Network Toolbox in MATLAB [42].

6.2 ANN development

The input fatigue damage indices are used to train the ANNs. Other features, such as the size and location of the crack are also included in the ANNs. In Table 4, the details of the ANNs are explained. A total of 25 neurons are utilized for the 2 hidden layers. With a learning rate of 0.01, around 1000 epochs were used to obtain the desired responses. In Fig. 12, the correlation curves are shown for the training, testing, and entire input data sets, with circles representing the magnitude of the estimated damage indices. In this figure, the dashed line represents the ideal correlation. A linear fit is shown in the colored lines, which represents the minimized least squares error for the predicted fatigue damage indices. It can be observed that the estimated correlation line is superimposed on ideal correlation, which demonstrates the accuracy of the ANN-based regression in detecting cracks. The applied data for training, validation, and testing are extracted from different groups, as previously discussed.

The ANNs are trained, validated, and tested by the fatigue damage indices inputs for the healthy and cracked (damaged) condition of the gusset-less connection. In this section, the crack detection results of the ANNs are discussed. The ANN results demonstrated that the healthy fatigue damage indices of the five strain rosettes have a unique correlation, which can be utilized as the criterion for fatigue crack detection. This correlation between the responses may not be valid for unhealthy fatigue damage indices. The deviance from the healthy condition is significantly influenced by the crack size, location, and distance to the installed sensors. Therefore, depending on these crack properties, one or more strain rosettes may not follow the existing correlation for healthy condition. The observed difference can be used as a tool to estimate the crack location [43, 45].

6.2.1 Crack properties' influence on damage detection

In Fig. 13, the ANN results for fatigue crack detection at the five strain rosettes are shown for the investigated crack

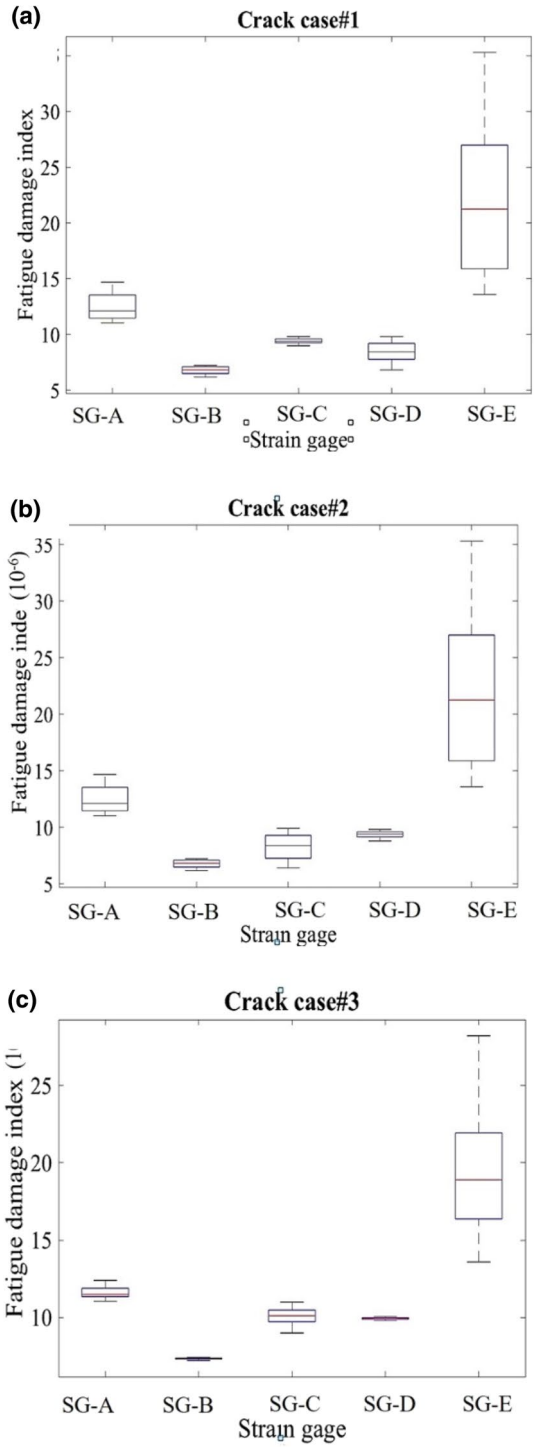

Fig. 11 Variability of the measured fatigue damage indexes with multiple crack sizes for **a** crack case#1, **b** crack case#2, **c** crack case#3

cases. The damage detection results are expressed through p values. The null hypothesis, H_0, is defined when the correlation between the fatigue damage indices remains unchanged [44]. The p value results range from 0 to 1, ranging from completely expected to unexpected results, respectively.

Table 3 Data inputs for training ANN

Health conditions of the component	Crack induced stress cycles (%)	Training	Validation	Test
Healthy	0	400	100	100
Healthy/cracked	50	200	50	50
Cracked	100	300	50	50

Any calculated p value is evaluated with the "significant level" parameter, α. The p values below α denotes the H_0 is rejected, while for the p values above α, H_0 cannot be rejected [46]. In this study, α is considered as 0.005.

As shown in Fig. 13, Crack 1 is located at the left curved weld of the gusset-less connection, which is close to SG-A. At early crack sizes, the correlation of the five responses does not change, while larger crack sizes only impact SG-A. The crack subsequently changes the correlation at SG-E, SG-C, SG-D, and SG-B. Crack 2 is simulated close to SG-E, which is detected to be a smaller size fatigue crack compared to Crack 1. SG-A, SG-B, SG-C have the largest distance to the simulated Crack 2 and may less effectively provide information about early-stage crack growth at the curved weld toes. Crack 3 does less significantly change the correlation between the fatigue damage indices, though some change is observed at larger crack sizes, as compared to Cracks 1 and 2. Therefore, Crack 3 is first detected via SG-E and is subsequently detected through other sensors at very large crack sizes, when the concentrated stresses are transferred to the web of the gusset-less connection.

The crack detection results demonstrated the importance of having a sufficient sample of crack-induced fatigue damage indices for training. Therefore, simulating multiple fatigue crack cases via the FE model and providing sufficient fatigue damage indices for training can enhance the efficacy of the fatigue crack detection algorithm. Additionally, since crack propagation in steel bridges occurs under variable loading conditions, it is essential to investigate the impact of variable cyclic loading on fatigue crack predictions made via ANNs.

6.2.2 Loading conditions' influence on damage detection

In this section, fatigue crack detection performance via the ANNs is investigated, considering the impact of variable loading conditions. Fatigue damage indices under different traffic scenarios are compared with the ANN results. In addition, fatigue damage indices of the healthy structure were considered to evaluate the possibility of false positive results through the ANNs [47]. It is noteworthy that different traffic scenarios were used for validation and for training the ANNs. In Fig. 14, the fatigue crack detection results are shown for multiple crack tip stress ranges for

Table 4 Summary of ANN properties

	ANN parameter
Number of neurons	25
Type of back propagation	Levenberg–Marquardt
Activation function	Sigmoid function
Learning rate	0.01
Training mode	Batch mode

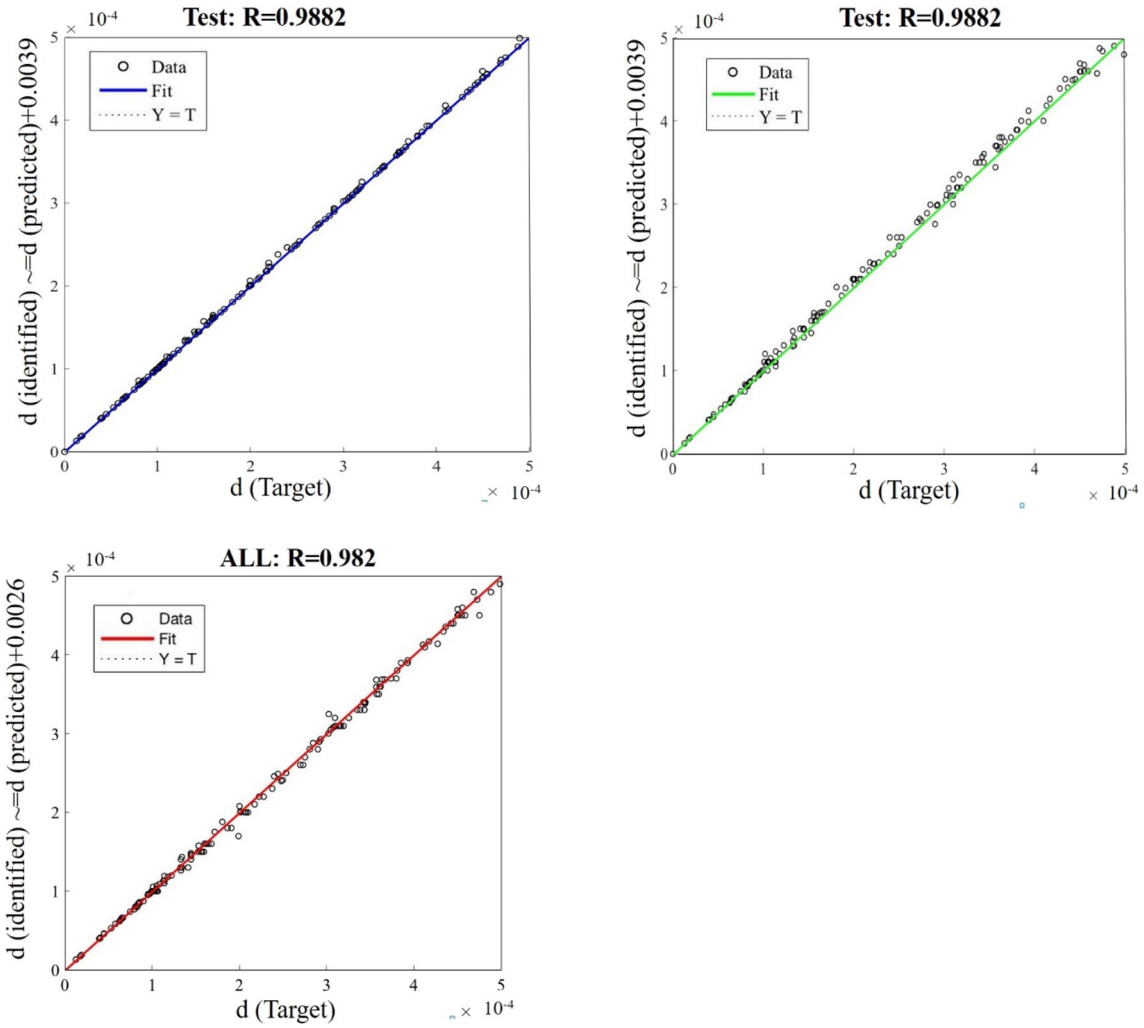

Fig. 12 Correlation between artificial neural network output and target values for training, validation, and testing inputs

the three cracked cases. It can be observed that the error in prediction of crack-induced fatigue indices increases for the less frequent stress cycles. These stress amplitudes are below the threshold required for crack opening, which is shown for the 15 MPa stress ranges in Fig. 14. The fatigue damage indices from scenarios 5 to 8 have more significant amplitudes, which can cause crack propagation, but they also have lower frequency (cycles). Therefore, the fatigue damage indices of unhealthy conditions are required to be estimated for above threshold stress ranges.

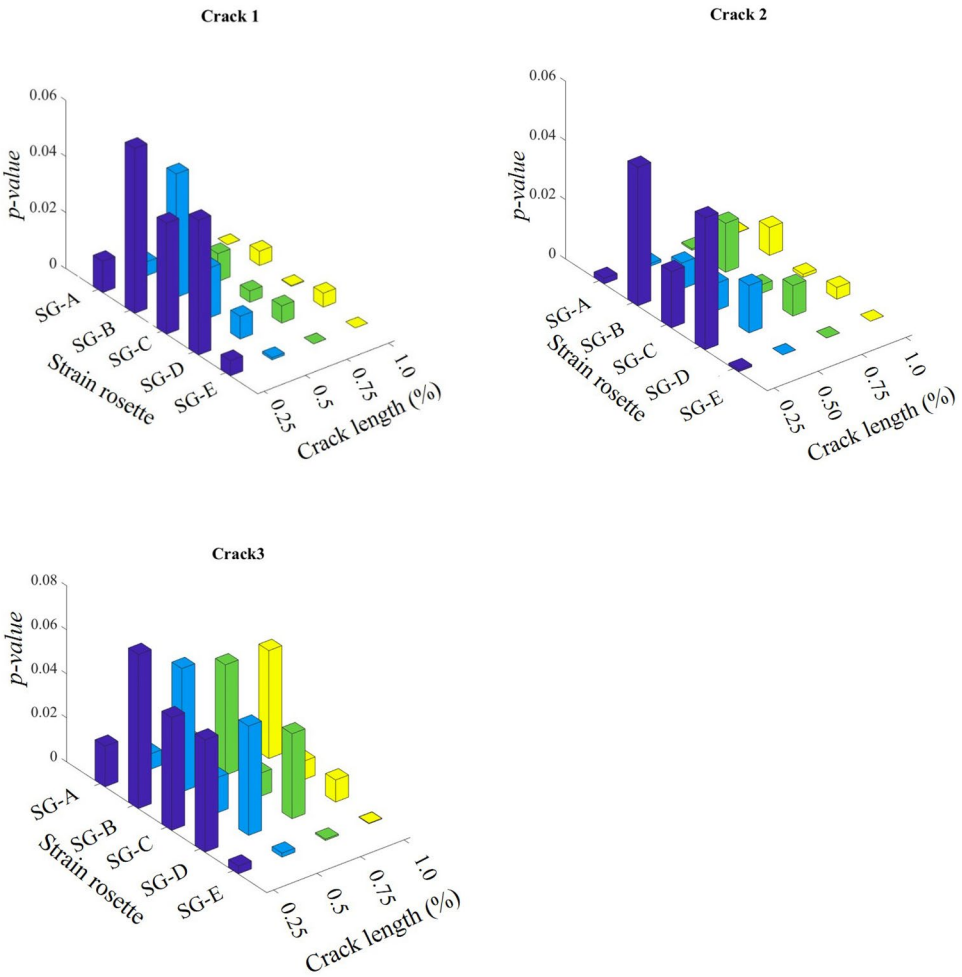

Fig. 13 Crack detection in five strain rosettes vs. crack lengths for three crack cases

6.2.3 Minimum crack size detection via the ANN model

In this study, the minimum size of a fatigue crack, which can be captured through an array of strain rosettes, is determined using the trained ANNs. A possible fatigue crack may be detected via one or more strain rosettes, depending on the crack properties and instrumentation system of the structural component. In Fig. 15, the minimum detected crack size is shown for the five installed strain rosettes and the three crack cases. SG-E is shown to be more sensitive to the defined crack cases and has a significant impact on the correlation between the fatigue damage indices of the five strain rosettes locations. It is also seen that the fatigue damage index of strain rosettes SG-B and SG-D may not considerably influence the correlation of fatigue damage indices. This result can be due to the relatively large distance of the strain rosettes to the damage locations.

It is also shown that Crack 3 may not be predicted when using only the SHM data of the strain rosettes for training the ANNs, because it is located on the other side of the connection. The results confirm that even excessive numbers of data acquisition system might not warrant early damage detection if they are not installed at appropriate positions. Indeed, this is a well-understood fact that the responses measured by a sensor network must have a sensitivity to the damage scenarios of interest. In this case, the success of early-stage fatigue crack prediction is dependent on the instrumentation plan, including the quantity and the location of the sensors.

7 Conclusion

In this study, an ANN-based algorithm is utilized to detect initiated fatigue cracks in complex welded components of steel bridges by using a sensor network and a high-fidelity computational model. The SHM and numerical strain responses of a case-study welded component, the gusset-less connection of the Memorial Bridge, were utilized to estimate the fatigue damage index of the investigated structural component. Fatigue damage index was the primary input for training the ANN, which allows integrating SHM data with numerical data of a validated FE model. Additional inputs consisted of environmental data, such as wind speed

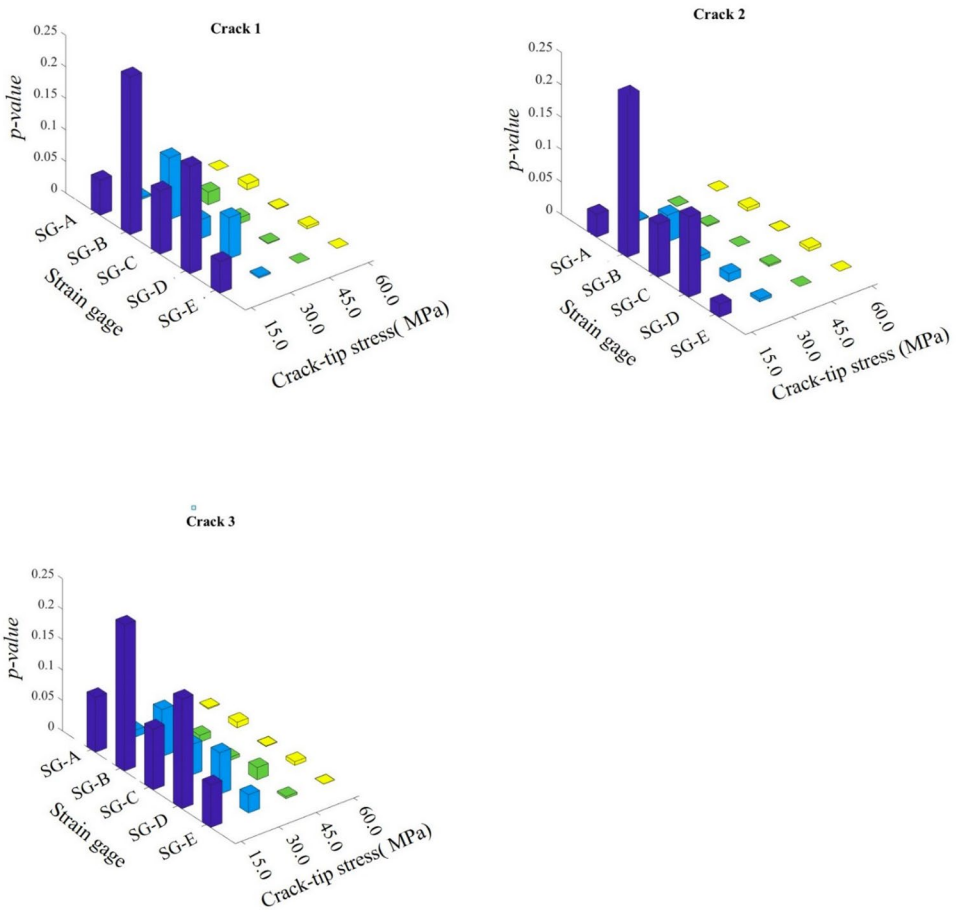

Fig. 14 Crack detection vs. crack tip stresses in five strain rosettes for three crack cases

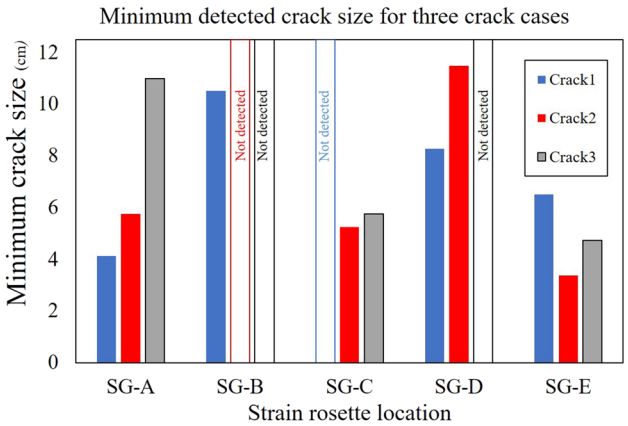

Fig. 15 Minimum detected crack size detected using the ANN models of the five strain rosettes for three crack cases

and temperature. Furthermore, a multiscale FE model of the case-study bridge was utilized to obtain crack tip stress time histories under the simulated dominant traffic loads of the bridge. It was demonstrated that the fatigue damage index, which reflects crack tip stress variations, is an appropriate input for damage detections utilizing ANNs. The efficacy of the ANN inputs was illustrated through more successful damage detection results. The following concluding remarks were also deduced from the damage detection results:

1. The applied multiscale FE model provide the opportunity to obtain time-history stress responses at the simulated crack tip, which can be more compatible with the field data. The local FE models of damaged components only show crack tip stresses, under constant amplitude stress. This multiscale model also allowed simulating the geometry of fatigue cracks via three-dimensional shell elements. Also, the FE model can provide additional stress results at non-instrumented locations of the component to address the restriction of insufficient instrumentation. Other useful numerical stresses include stress from unexpected traffic conditions and progressive damages that may occur in the future service life of the bridges.
2. The included environmental data for training ANN were shown to have a significant impact for damage detection if SHM data are used as inputs. The environmental changes may not directly impact the estimated fatigue damage indices, while they can describe the traffic

changes and, the resulting stresses, which are reflected in the estimated fatigue damage indices. Using this environmental information allows ANNs to differentiate the variation of the stresses due to traffic changes from damaged stress results.

3. Damage detection and localization with this method report general trends of bridge performance. Therefore, the proposed damage detection program assists the management system of bridges with in-demand inspections and provides fatigue life degradations of the structural components of the bridges over the designated service lives.
4. In this study, it was shown that the combination of monitoring data and a physics-based model facilitates detecting, locating, and characterizing the fatigue damage. Without the use of a physics-based model, it is unlikely to characterize the damage.

Acknowledgements This material is based upon work partially supported by the National Science Foundation under Grant No. 1430260, FHWA AID: DEMO Program and funding from the NHDOT Research Advisory Council. Any opinions, findings, and conclusions or recommendations expressed in this material are those of the author(s) and do not necessarily reflect the views of the National Science Foundation. The research team is also grateful to HNTB Corporation, in particular, Ted Zoli, for sharing design information on the Memorial Bridge.

References

1. Farrar CR, Worden K (2012) Structural health monitoring: a machine learning perspective. Wileya, New York
2. Sohn H, Farrar CR, Hunter NF, Worden K (2001) Structural health monitoring using statistical pattern recognition techniques. J Dyn Syst Meas Control Spec Issue Identif Mech Syst 123(4):706–711. https://doi.org/10.1115/1.1410933
3. Fisher JW, Roy S (2015) Fatigue damage in steel bridges and extending their life. Adv Steel Res (Adv Steel Constr) 11(3):250–268
4. Leander J (2013) Refining the fatigue assessment procedure of existing steel bridges. Ph.D. Dissertation. Stockholm: KTH Royal Institute of Technology, 2013
5. Adeli H (2001) Neural networks in civil engineering. Comput Aided Civ Infrastruct Eng 16(2):126–142. https://doi.org/10.1111/0885-9507.00219
6. Catbas FN, Susoy M, Frangopol DM (2008) Structural health monitoring and reliability estimation: long span truss bridge application with environmental monitoring data. Eng Struct 30(9):2347–2359
7. Ghannadi P, Kourehli SS (2019) Data-driven method of damage detection using sparse sensors installation by SEREP. J Civ Struct Health Monit 9(4):459–475. https://doi.org/10.1007/s13349-019-00345-8
8. Amezquita-Sanchez JP, Adeli H (2015) Feature extraction and classification techniques for health monitoring of structures. Sci Iran 1931–1940
9. Gu J, Gul M, Wu X (2017) Damage detection under varying temperature using artificial neural networks. Struct Control Health Monit. 24(11):e1198
10. EftekharAzam S, Rageh A, Linzell D (2019) Damage detection in structural systems utilizing artificial neural networks and proper orthogonal decomposition. Struct Control Health Monit 26(2):e2288. https://doi.org/10.1002/stc.2288
11. Azimi M, DadrasEslamlou A, Peckan G (2020) Data-driven structural health monitoring and damage detection through deep learning: state-of-the-art review. Sensors 20(10):2778. https://doi.org/10.3390/s20102778
12. Karimian SF, Moradi R, Cofre-Martel S, Groth KM, Modarres M (2020) Neural network and particle filtering: a hybrid framework for crack propagation prediction. Signal Process 2004
13. Kang J, Hoi B, Lee K, Kim J, Kim K (2006) Neural network application in fatigue damage analysis under multiaxial random loadings. Int J Fatigue 28(2):132–140
14. Fathalla E, Tanaka Y, Maekawa K (2018) Remaining fatigue life assessment of in-service road bridge decks based upon artificial neural networks. Eng Struct 171:602–616. https://doi.org/10.1016/j.engstruct.2018.05.122
15. Durodola JF, Ramachandra S, Gerguri S et al (2018) Artificial neural network for random fatigue loading analysis including the effect of mean stress. Int J Fatigue 111:321–332
16. Zhan Z, Li H (2021) Machine learning based fatigue life prediction with effects of additive manufacturing process parameters for printed SS 316L. Int J Fatigue 142:105941. https://doi.org/10.1016/j.ijfatigue.2020.105941
17. Rageh A, Azam SE, Linzell DG (2020) Steel railway bridge fatigue damage detection using numerical models and machine learning: mitigating influence of modeling uncertainty. Int J Fatigue 134:105458. https://doi.org/10.1016/j.ijfatigue.2019.105458
18. Yan F, Chen W, Lin Z (2016) Prediction of fatigue life of welded details in cable-stayed orthotropic steel deck bridges. Eng Struct 127:344–358. https://doi.org/10.1016/j.engstruct.2016.08.055
19. Leander J (2018) Fatigue life prediction of steel bridges using a small scale monitoring system. Stockholm. http://urn.kb.se/resolve?urn=urn:nbn:se:kth:diva-238718.
20. Xu Y, Bao Y, Chen J, Zuo W, Li H (2019) Surface fatigue crack identification in steel box girder of bridges by a deep fusion convolutional neural network based on consumer-grade camera images. Struct Health Monit 18:653–674
21. Wang B, Xie L, Song J, Zhao B, Li C, Zhao Z (2021) Curved fatigue crack growth prediction under variable amplitude loading by artificial neural network. Int J Fatigue 142:105886. https://doi.org/10.1016/j.ijfatigue.2020.105886
22. Downing SD, Socie DF (1982) Simple Rainflow counting algorithms. Int J Fatigue 4(1):31–40
23. Miner MA (1945) Cumulative damage in fatigue. J Appl Mech 12(3):A159–A164
24. AASHTO (2017) ASHTO LRFD bridge design specifications, 8th edn. AASHTO, Washington, DC
25. Paris P, Erdogan F (1963) A critical analysis of crack propagation laws. J Basic Eng 85(4):528–533
26. Guo T, Li A, Wang H (2008) Influence of ambient temperature on the fatigue damage of welded bridge decks. Int J Fatigue 30(6):1092–1102. https://doi.org/10.1016/j.ijfatigue.2007.08.004
27 Chiewanichakorn M, Aref AJ, Alampali S (2007) Dynamic and fatigue response of a truss bridge with fiber reinforced polymer deck. Int J Fatigue 29:1475–1489
28. Waszczyszyn Z (1999) Fundamentals of artificial neural networks. In: Waszczyszyn Z (ed) Neural networks in the analysis and design of structures. Springer, Vienna, pp 1–51
29. Gope D, Gope PC, Thakur A, Yadav A (2015) Application of artificial neural network for predicting crack growth direction in multiple cracks geometry. Appl Soft Comput 30:514–528
30. Adams T, Mashayekhizadeh M, Santinni-Bell E, Wosnik M, Baldwin K, Fu T (2017) Structural response monitoring of a

vertical lift Truss Bridge. In: 96th Annual Meeting. Transportation Research Board, Washington, D.C.
31. Mashayekhizadeh M, Santini-Bell E, Adams T (2017) Instrumentation and structural health monitoring of a vertical lift bridge. Processings of 27th ASNT Research Symposuim, Jacksonville
32 Alampalli S, Ettouney MM, Agrawal AK (2005) Structural Health Monitoring for Bridge Maintenance. Bridge Struct 1:345–354
33. Mashayekhi M, Santini-Bell E (2018) Three-dimensional multi-scale finite element models for in-service performance assessment of bridges. Comput Aided Civil Infrastruct Eng 34(5):385–401
34. Shahsavari V, Mashayekhi M, Mehrkash M, Santini-Bell E (2019) Diagnostic testing of a vertical lift truss bridge for model verification and decision-making support. Front Built Environ (Front) 5:92. https://doi.org/10.3389/fbuil.2019.00092
35. Mashayekhi M, Santini-Bell E (2020) Fatigue assessment of a complex welded steel bridge connection utilizing a three-dimensional multi-scale finite element model and hotspot stress method. Eng Struct 214:110624. https://doi.org/10.1016/j.engstruct.2020.110
36. Rageh A, Linzell DG, EftekharAzam S (2018) Automated, strain-based, output-only bridge damage detection. J Civil Struct Health Monit 8:833–846. https://doi.org/10.1007/s13349-018-0311-6
37 Tchemodanova SP, Mashayekhi M, Sanayei M, Santini Bell E (2021) Multiaxial fatigue assessment of complex steel connections: a case study of a vertical-lift gussetless truss bridge. Eng Struct 235:111996
38. Agathos K, Chatzi E, Bordas SPA, Talaslidis D (2016) A well-conditioned and optimally convergent XFEM for 3D linear elastic fracture. Int J Numer Methods Eng 105(9):643–677
39. Belytschko T, Black T (1999) Elastic crack growth in finite elements with minimal remeshing. Int J Numer Methods Eng 45:601–620
40. Chena D, Lib G, Wangb Y, Xiaoa Q (2019) Research on fatigue crack propagation of a T-joint based on XFEM and TSA. Eng Fract Mech 222:106707. https://doi.org/10.1016/j.engfracmech.2019.106707
41. Barsom, J. 1976. Fatigue crack growth under variable-amplitude loading in various bridge steels. In: Wei R, Stephens R (eds) Fatigue crack growth under spectrum loads, pp 217–232. ASTM International, West Conshohocken. https://doi.org/10.1520/STP33374S
42. Bucar T, Nagode M, Fajdiga M (2006) A neural network approach to describing the scatter of S-N curves. Int J Fatigue 28:311–323
43. MathWorks (2017) Create, train, and simulate shallow and deep learning. https://www.mathworks.com/products/neural-network.html
44. Neves AC, González I, Leander J, Karoumi R (2017) Structural health monitoring of bridges: a model-free ANN-based approach to damage detection. J Civil Struct Health Monit 7:689–702. https://doi.org/10.1007/s13349-017-0252-5
45 Abedin M, Mehrabi AB (2019) Novel approaches for fracture detection in steel girder bridges. Infrastructures 4:42
46 Weinstein JC, Sanayei M, Brenner BR (2018) Bridge damage identification using artificial neural networks. J Bridge Eng. https://doi.org/10.1061/(ASCE)BE.1943-5592.0001302
47. Nguyen D, Widrow B (1990) Improving the learning speed of 2-layer neural networks by choosing initial values of the adaptive weights. 1990 IJCNN International Joint Conference on Neural Networks, 1990, pp 21–26, vol 3. https://doi.org/10.1109/IJCNN.1990.137819